Journal of *Marine Science and Engineering*

MDPI

Article

Formation Mechanism of Heavy Hydrocarbon Carbon Isotope Anomalies in Natural Gas from Ordovician Marine Carbonate in the Ordos Basin

Wen Zhang [1], Wenhui Liu [1,*], Xiaofeng Wang [1], Zhengliang Huang [2], Qingfen Kong [2], Houyong Luo [1], Dongdong Zhang [1], Peng Liu [3], Xiaoyan Chen [1] and Zhenghong Cai [2]

[1] State Key Laboratory of Continental Dynamics, Department of Geology, Northwest University, Xi'an 710069, China; wenwenmma@163.com (W.Z.); wangxf@nwu.edu.cn (X.W.); luohouyongg@nwu.edu.cn (H.L.); zhangdd@nwu.edu.cn (D.Z.); chenxiaoyan180401@163.com (X.C.)
[2] Research Institute of Exploration and Development, PetroChina Changqing Oilfield, Xi'an 710018, China; hzl0915_cq@petrochina.com.cn (Z.H.); kqf_cq@petrochina.com.cn (Q.K.); caizh_cq@petrochina.com.cn (Z.C.)
[3] College of Safety Science and Engineering, Xi'an University of Science and Technology, Xi'an 710054, China; pengliu@xust.edu.cn
* Correspondence: whliu@nwu.edu.cn

Abstract: Interactive depositional systems of marine carbonates and gypsum salt rocks are closely related to natural gas reservoirs. Despite continuous progress in the exploration of new areas of marine carbonate genesis within the Ordos Basin, the source and mechanism of "sub-salt" natural gas genesis remains controversial. In this study, we investigated natural gas genesis through geochemical analysis of Lower Paleozoic natural gas samples from the mid-eastern Ordos Basin, obtaining natural gas composition data and carbon/hydrogen isotope compositions. We found evident differences between the geochemical characteristics of "sub-salt" and "post-salt" natural gas; the methane carbon isotope signature of "sub-salt" natural gas was lighter overall than that of "post-salt" natural gas, while the ethane carbon isotope composition of the former was more widely distributed and partially lighter than that of the latter. Combining these data with the regional geological background and existing geochemical data, it is evident that Ordovician "post-salt" natural gas comprises a composite of Upper Paleozoic coal-type gas and Lower Paleozoic oil-type gas, with the oil-type gas accounting for the largest proportion. In contrast, the "sub-salt" natural gas was formed and preserved within the Ordovician marine carbonates or sourced from deeper and more ancient hydrocarbon source rocks. Geochemical anomalies, including light methane carbon isotopes and ethane carbon isotopes with coal-type gas characteristics, are closely related to the prevalence of thermochemical sulfate reduction during hydrocarbon formation and reservoir formation of natural gas in "sub-salt" strata.

Keywords: Majiagou Formation; thermochemical sulfate reduction; marine carbonate rock; Ordos Basin

Citation: Zhang, W.; Liu, W.; Wang, X.; Huang, Z.; Kong, Q.; Luo, H.; Zhang, D.; Liu, P.; Chen, X.; Cai, Z. Formation Mechanism of Heavy Hydrocarbon Carbon Isotope Anomalies in Natural Gas from Ordovician Marine Carbonate in the Ordos Basin. *J. Mar. Sci. Eng.* **2023**, *11*, 2176. https://doi.org/10.3390/jmse11112176

Academic Editor: Timothy S. Collett

Received: 14 October 2023
Revised: 10 November 2023
Accepted: 12 November 2023
Published: 15 November 2023

1. Introduction

The Ordos Basin is one of the key basins for marine carbonate oil and gas exploration in China [1]. Since the discovery of natural gas reservoirs in Upper Ordovician weathering crusts in 1989, there has been continuous exploration and a series of new discoveries [2]. However, the focus has previously been on exploring weathering crust-related natural gas in the Lower Paleozoic Majiagou Formation, and the "sub-salt" stratigraphy of the Majiagou Formation is still in the stage of continuous exploration [3]. In 2021, the eastern exploration well, Mitan-1, obtained high-yield industrial gas flow in the fourth member of the Majiagou Formation, signaling a new phase of "sub-salt" gas exploration in the eastern part of the basin [4].

However, current geochemistry-related studies on the natural gas components, carbon and hydrogen isotope compositions, and other geochemical correlations are insufficient for

the in-depth exploration of the "sub-salt" gas reservoir ($Ma5_6$–Ma1). Controversy remains surrounding the source and mechanism of genesis; some scholars suggest that the "sub-salt" natural gas may come from the marine hydrocarbon source rock of the Majiagou Formation (i.e., formed and preserved in this formation without transport) [5], while others argue that Lower Paleozoic oil-type gas mixed with Upper Paleozoic coal-type gas to form the Ordovician natural gas [6]. However, there is currently no qualitative understanding as to which point of view is correct.

In this study, Ordovician natural gas samples from the mid-eastern part of the Ordos Basin were analyzed to obtain their natural gas components, along with their alkane carbon and hydrogen isotope compositions. Using these data combined with existing natural gas geochemical data from the region, this contribution comprehensively discusses the sources and genesis of Ordovician natural gas in the mid-eastern part of the basin and integrates the regional geological tectonic background and characteristics of hydrocarbon source rocks. Through discussion of the heavy hydrocarbon carbon isotope anomalies of the Ordovician "sub-salt" natural gas in the Lower Paleozoic strata of the Ordos Basin, this study helps to clarify the indicators of different sources of Paleozoic natural gas in the basin; at the same time, it provides a scientific basis for further exploration and resource evaluation of deep natural gas.

2. Geological Background

2.1. General Geology

The Ordos Basin is located in central China (Figure 1), bordered by the Yinshan Mountains to the north, Qinling Mountains to the south, Luliang Mountains to the east, and Helan Mountains to the west. It is approximately rectangular in shape, being broad and shallow in the east, steep and narrow in the west, and asymmetrical in the north–south direction [7]. It contains six first-order tectonic units, i.e., Yimeng uplift, Western margin thrust belt, Tianhuan depression, Yishan slope, Jinxi fault–fold belt, and Weibei uplift. Among these, the Yishan slope is a westerly dipping, gently sloping, monoclinal structure, comprising the main area of oil and gas enrichment [8]. During the Early Paleozoic, the Ordos Basin was part of the epeiric sea of the North China Platform. The Weibei uplift developed in the southern part of the basin, and the Yimeng uplift developed in the northern part. A paleo-uplift formed in the central part of the basin, distributed in an "L" shape towards the north and south. This played a decisive role in controlling the separation of the North China epeiric sea and Qinqi trough. The western area of the central paleo-uplift mainly experienced carbonate rock deposition, and the eastern area experienced carbonate and gypsum salt rock deposition [9].

The Ordos Basin developed two sets of gas-bearing assemblages in the Paleozoic: Upper Paleozoic (Carboniferous–Permian) tight sandstone gas reservoirs and Lower Paleozoic (Ordovician) carbonate gas reservoirs [10]. The hydrocarbon source rocks of the Carboniferous–Permian tight sandstone gas reservoirs are coal and dark mudstone, which are relatively uniformly distributed within the basin; these are the main hydrocarbon source rocks of the basin and are relatively thin in the central part of the basin and thicken towards the west and east [11]. The coal-derived hydrocarbon rocks have entered a high maturity stage in most parts of the basin, with an overall trend of relatively low maturity in the north and east and relatively high maturity in the south and west. The mechanism of natural gas formation and storage is relatively evident; the gas has either been generated and preserved within these Carboniferous–Permian strata or generated in older strata and transported to these younger strata at a later stage [12].

The Ordovician marine carbonate gas reservoirs can be divided into two sets of gas-forming assemblages, "post-salt" and "sub-salt", based on the high-quality isolated gypsum rocks of the fifth sub-member in the fifth member of the Majiagou Formation ($Ma5_5$). The "post-salt" assemblage ($Ma5_{1–5}$) mainly comprises paleokarst weathering crust-type gas reservoirs. After tectonic uplift by the Caledonian movement, well-developed gas storage space under long-term rock dissolution effects and direct contact between Upper Paleozoic

coal-gas source rocks and the erosion surface of the weathering crust formed a geological background conducive to Upper Paleozoic coal-gas transport and formation of reservoirs therein [13]. According to previous research, the main body of the gas source is considered to have been generated in newer formations and transported to older formations at a later stage to accumulate into natural gas reservoirs, but the contribution of a Lower Paleozoic marine gas source cannot be excluded [14].

Considering that the formation and evolution mechanisms of Paleozoic natural gas in different regions of the Ordos Basin are different, the study area is divided into three zones. Zone A contains the Sulige and Wuxingqi gasfields, together with the northern part of the Jingbian gasfield. Under the influence of the central paleo-uplift, this block developed large-scale karst carbonate reservoirs, which are in direct contact with the overlying coal source rocks. Zone B comprises the southern part of the Jingbian gasfield, and this area has experienced a large burial depth. The Paleozoic coal-measure source rocks and carbonate source rocks have reached a high evolution stage. At the same time, the thickness of the gypsum layer here is small, which provides a good condition for the vertical migration of natural gas. Zone C comprises the Shenmu, Yulin, Mizhi, and Zizhou gasfields, and the main body of this area is the Mizhi salt lake. Here, the evolution degree of Paleozoic coal-measure and carbonate source rocks is lower than that of zones A and B. The gypsum salt layers of the Majiagou Formation are very thick in this zone, and the "post-salt" and "sub-salt" reservoirs are separated by thick gypsum salt to form relatively independent gas-bearing systems. Meanwhile, thin carbonate source rocks are also present under the salt. The thickness of a single layer is small, but the overall thickness is large, which meets the geological conditions for gas reservoirs formed and preserved in situ. The study area is constrained by the ancient basement structure, lithofacies paleogeography, and karst paleogeomorphology. Zone A was influenced by the confined sea in the north, while zone B was influenced by the open sea in the south; at the end of the Huaiyuan Movement, the central paleo-uplift began to rise, and a large-scale restricted intra-platform depression formed. Overall, this resulted in a pattern of thin gypsum salt rocks in the south and thicker gypsum salt rocks in the north.

2.2. Petroleum Systems

There are two sets of natural gas source rocks in the Ordos Basin, i.e., Upper Paleozoic (Carboniferous–Permian) transitional coal-measure-clastic rocks and Lower Paleozoic (Ordovician) marine carbonate rocks.

Sea level in the eastern part of the Ordos Basin during the Early Ordovician Majiagou Stage exhibited cyclic rises and falls, leading to a sedimentary structure of carbonate rocks interbedded with gypsum [15]. The thickness of the carbonate–gypsum salt sedimentary system of the Majiagou Formation is approximately 100–900 m. It exhibits cyclic superposition vertically and is divided into six sections from bottom to top (Ma1–Ma6) [3]. Among these, the lithology of the Ma1, Ma3, and Ma5 members is dominated by gypsum and evaporated tidal flat dolomite, representing the evaporative environment of a restricted sea during a period of recession. The Ma2, Ma4, and Ma6 members are dominated by carbonate rocks, with a small amount of locally interbedded anhydrite representing an environment that was essentially connected to the main seawater body during a period of transgression [16]. The Majiagou Formation is further sub-divided into 10 sub-sections according to the relative rise and fall in sea level (from bottom to top, $Ma5_1$–$Ma5_{10}$). Of these, the Ma56 sub-member represents the main evaporite development period in the Majiagou Formation; it has a large depositional thickness and wide distribution and serves as a dividing line separating the Majiagou Formation into a "post-salt" gas-bearing assemblage ($Ma5_1$–$Ma5_5$) and "sub-salt" gas-bearing assemblage ($Ma5_6$–Ma1) [9].

At the end of the Early Ordovician, the mid-eastern part of the basin entered a period of tectonic uplift controlled by the Caledonian Movement and experienced weathering and denudation for 130–150 million years. Widely developed weathering-crust karstic dolomite reservoirs formed at the top of the Ordovician strata [17]. The organic-rich

lithologies among the Lower Paleozoic marine hydrocarbon source rocks are mainly thinly bedded mudstone interlayers and medium–thinly bedded muddy dolomites [9]. The organic matter includes kerogen, abundant soluble organic matter, and acid-soluble organic matter [18], with a high conversion rate of hydrocarbon production. The sedimentary strata comprising thick layers of gypsum salt rocks in the Ma1, Ma3, and Ma5 members have horizontal continuity, wide distribution range, and large scale, making them favorable capping layers for natural gas reservoirs in this gypsum–carbonate rock sedimentary system. This has particular significance for natural gas aggregation in the large zone of dolomite beneath the gypsum and in the thin interlayers of dolomite developed among the gypsum salt rocks, laying a unique foundation for the oil and gas geochemistry of this distinct carbonate–gypsum salt stratigraphic system. During the Late Carboniferous Benxi Stage, the Ordos Basin entered a further period of tectonic subsidence, leading to the formation of extensive coal-bearing sedimentary strata in sea–land transition and shoreline swamp environments. The Carboniferous–Permian coal strata are characterized by extensive overburden deposition and are in widespread and direct contact with the weathering crust reservoirs of the Upper Ordovician [19].

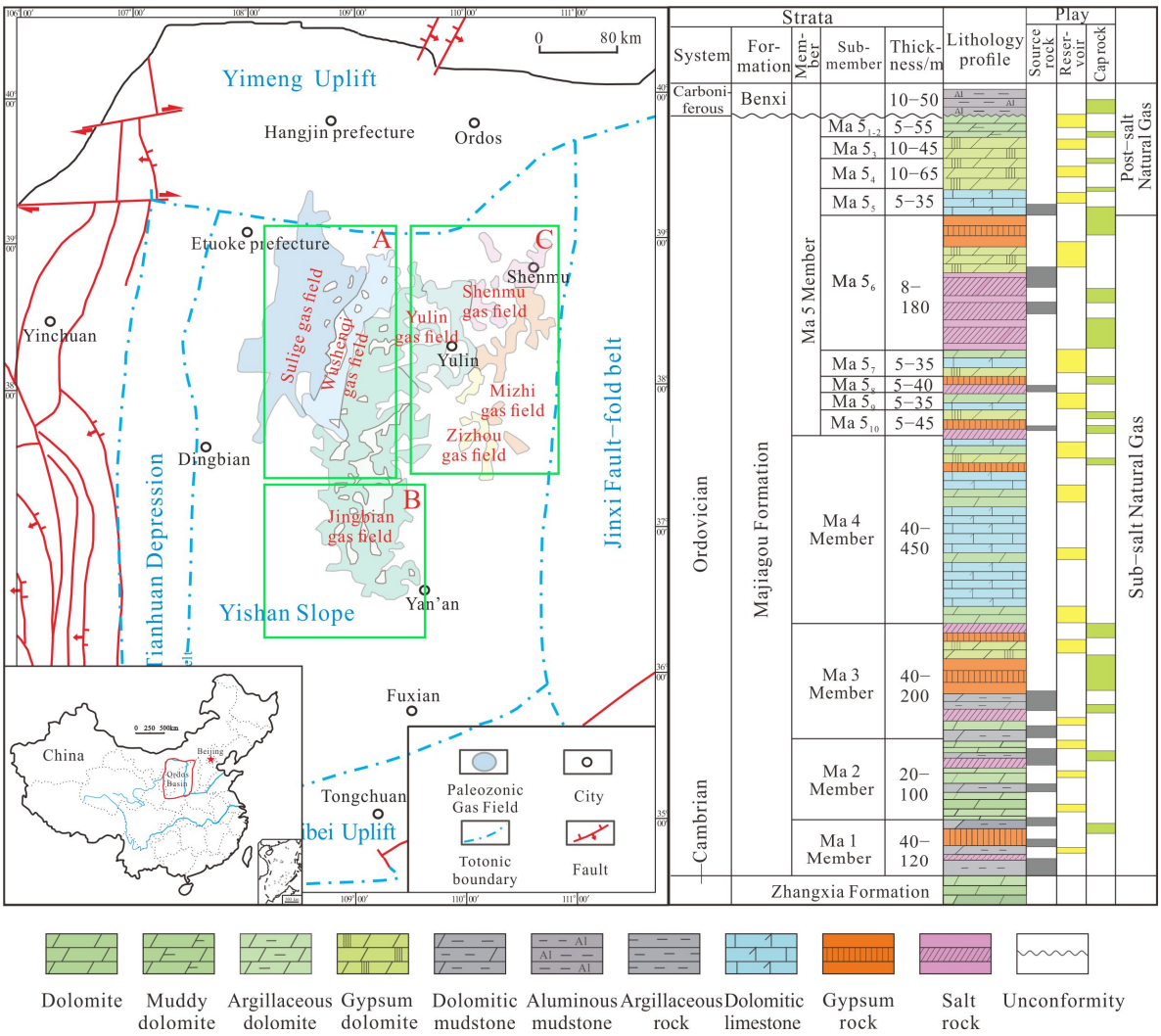

Figure 1. Structural diagram and comprehensive stratigraphic column of the Ordos Basin.

3. Samples and Experiments

3.1. Samples

The natural-gas-producing formations in the Ordos Basin are mainly found in the Carboniferous–Permian Shihezi, Shanxi, Taiyuan, and Benxi formations and the Ordovician Majiagou Formation. Among these, there are abundant gas wells and relevant published data for the Carboniferous–Permian and Ordovician "post-salt" horizons, while the development and exploration level of the "sub-salt" horizon of the Majiagou Formation is relatively low, with limited gas samples and fewer relevant data available. In this study, systematic geochemical analyses of gas components, along with carbon and hydrogen isotope compositions, were carried out on 21 recently collected Ordovician natural gas samples (seven "sub-salt" and 14 "post-salt" samples); moreover, 155 existing Ordovician natural gas geochemical analyses were compiled for use in a comprehensive comparison.

3.2. Geochemical and Stable Isotope Analysis

3.2.1. Chemical Composition

The chemical components of natural gas samples were determined using an Agilent Technologies 7890B gas chromatograph (GC) equipped with a flame ionization detector (FID) [20]. The temperature of the GC oven was initially set to 80 °C for 2 min, then increased to 100 °C at a heating rate of 5 °C/min, then further increased to 290 °C at a rate of 10 °C/min and maintained for 3 min. All chemical compositions are shown in percent (%).

3.2.2. Stable Carbon Isotope Composition

The carbon and hydrogen isotope compositions of natural gas hydrocarbons were determined using a TRACE1300 GC (Thermo Fisher Scientific, Waltham, MA, USA) combined with a MAT-253 Plus mass spectrometer (Thermo Fisher Scientific, Waltham, MA, USA). The GC oven temperature was initially set to 80 °C for 3 min, then increased to 190 °C at a heating rate of 15 °C/min and maintained for 5 min. The combustion furnace temperature was 960 °C for carbon isotope analysis, and the cracking furnace temperature was 1350 °C for hydrogen isotope analysis. The $\delta^{13}C$ values are reported relative to Vienna Pee Dee Belemnite (VPDB) in permil (‰), with a measurement precision of ±0.3‰. The δD values are reported relative to Vienna Standard Mean Ocean Water (VSMOW) in permil (‰), with a measurement precision of ±5‰ [21].

4. Results

4.1. Geochemical Characterization of Natural Gas in Ordovician Carbonate Facies

4.1.1. Characteristics of Natural Gas Components

Natural gas is mainly composed of alkanes, of which CH_4 accounts for the majority, with small amounts of C_2H_6, C_3H_8, and C_4H_{10}. In addition to H_2S, CO_2, N_2, and H_2, a small amount of CO and trace amounts of rare gases, such as He and Ar, are generally also present.

The natural gas components of the Carboniferous–Permian coal-type gas in the mid-eastern region of the Ordos Basin were dominated by hydrocarbons; the methane content ranged from 72.65% to 97.49% (average 91.79%), ethane content ranged from 0.07% to 10.57% (average 4.15%) (Figure 2a), and dry coefficient ($C_1/\sum C_{1-5}$) ranged from 0.837 to 0.999 (average 0.946). The natural gas components of the Ordovician samples were also dominated by hydrocarbons; the methane content of the "post-salt" natural gas of the carbonate rocks ranged from 86.07% to 98.29% (average 94.91%), ethane content ranged from 0.06% to 2.69% (average 0.67%), and dry coefficient ranged from 0.968 to 0.999 (average 0.992). For the "sub-salt" natural gas samples, the methane content ranged from 45.37% to 97.86% (average 84.29%), ethane content ranged from 0.00% to 7.31% (average 1.36%), and dry coefficient ranged from 0.853 to 0.999 (average 0.978) (Table 1; Figure 2a). The non-hydrocarbon gases of the Ordovician natural gas were mainly CO_2 and N_2, and the content of H_2 was very low. The content of H_2S in some wells was high, up to 23.58%

(Figure 2b). Overall, the contents of CO_2 and N_2 increased evidently with the deepening of the horizon. In particular, some natural gas samples showed high CO_2 contents.

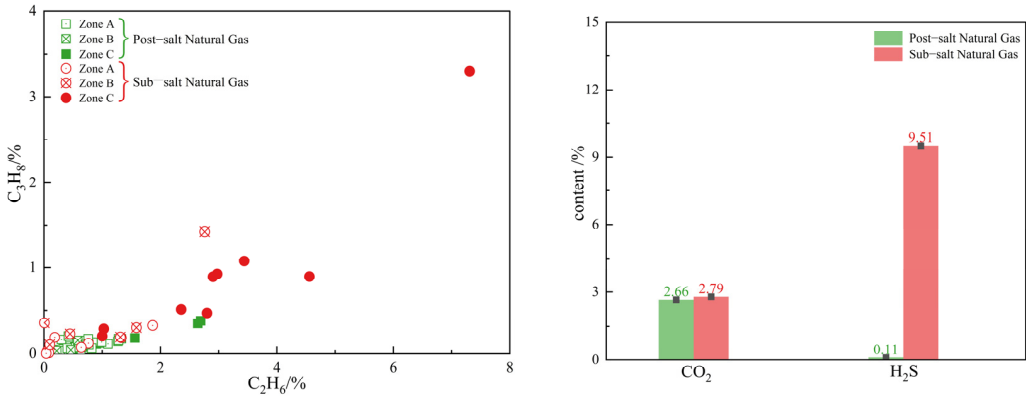

(**a**) (**b**)

Figure 2. Composition diagram of Lower Paleozoic natural gas in the Ordos Basin. (**a**) Correlation diagram of ethane−propane content. (**b**) Diagram of natural gas acid−gas content.

Table 1. Characteristics of Paleozoic natural gas fractions in the mid-eastern Ordos Basin.

Layer		Upper Paleozoic	Ordovician Post-Salt	Ordovician Sub-Salt
Hydrocarbon gas component/%	CH_4	72.65 ~ 97.49 / 91.79 (291)	86.07 ~ 98.29 / 94.91 (63)	45.37 ~ 97.86 / 84.29 (32)
	C_2H_6	0.07 ~ 10.57 / 4.15 (291)	0.06 ~ 2.69 / 0.67 (62)	0.00 ~ 7.31 / 1.36 (31)
	C_3H_8	0.01 ~ 3.68 / 0.83 (291)	0.01 ~ 0.38 / 0.09 (61)	0.00 ~ 3.30 / 0.50 (26)
	iC_4H_{10}	0 ~ 0.59 / 0.15 (221)	0.00 ~ 0.05 / 0.02 (31)	0.00 ~ 0.82 / 0.23 (17)
	nC_4H_{10}	0 ~ 0.92 / 0.16 (224)	0.00 ~ 0.05 / 0.02 (31)	0.00 ~ 0.81 / 0.15 (17)
Non-hydrocarbon gas components/%	CO_2	0.01 ~ 7.05 / 1.11 (227)	0.02 ~ 7.86 / 2.66 (60)	0.14 ~ 11.49 / 2.79 (29)
	N_2	0.03 ~ 22.23 / 1.66 (201)	0.02 ~ 12.01 / 1.61 (59)	0.17 ~ 52.04 / 6.24 (30)
	H_2S		0.05 ~ 0.13 / 0.11 (3)	0.28 ~ 23.58 / 9.51 (17)
	H_2	0.01 ~ 0.80 / 0.11 (24)		0.00 ~ 0.80 / 0.23 (5)
Dry coefficient		0.837 ~ 0.999 / 0.946 (291)	0.968 ~ 0.999 / 0.992 (62)	0.853 ~ 0.999 / 0.978 (32)
Data sources		This Study; Dai Jinxing, 2005, 2014 [22,23]; Yang Hua, 2009, 2015 [24,25]; Liu Quanyou, 2009, 2015 [26,27]; Xiao Hui, 2013 [28]; Zhang Wenzheng, 2016 [29]; Wang Ke, 2007 [30]; Hu Anping, 2007 [31]; Kong Qingfen, 2018 [32]; Xu Wanglin, 2019 [33]; Li Jian, 2018 [10]; Liu Erhu, 2022 [34]; Meng Qiang, 2023 [35].		

Minimum value−Maximum value / Average value (The number of samples).

4.1.2. Carbon Isotope Characteristics of Natural Gas

The carbon isotope-dominant frequency values of "post-salt" natural gas methane ranged from −40‰ to −30‰ (average −33.8‰), while the ethane carbon isotope values ranged from −36‰ to −22‰ (average −30.0‰), exhibiting a mixture of humic and rotten-mud characteristics. The carbon isotope-dominant frequency values of "sub-salt" natural gas methane ranged from −46‰ to −34‰ (average −37.8‰), while the ethane carbon isotope values ranged from −40‰ to −22‰ (average −29.4‰). In summary, the carbon isotope composition of methane was lighter, and the distribution range of ethane carbon

isotope composition was larger in "sub-salt" natural gas compared with "post-salt" natural gas.

The methane $\delta^{13}C$ signatures of the "sub-salt" natural gas were lighter than those of the "post-salt" natural gas; this is contrary to the normal evolutionary characteristics of homologous natural gas formation, reflecting the fact that they may have differences in source or secondary transformation. The ethane $\delta^{13}C$ signatures of the "sub-salt" natural gas had a wider range and were partially lighter than those of the "post-salt" natural gas. This reflects the different sources of the gases, also demonstrating the uniqueness and complexity of the formation and evolution mechanism of the "sub-salt" natural gas (Figure 3).

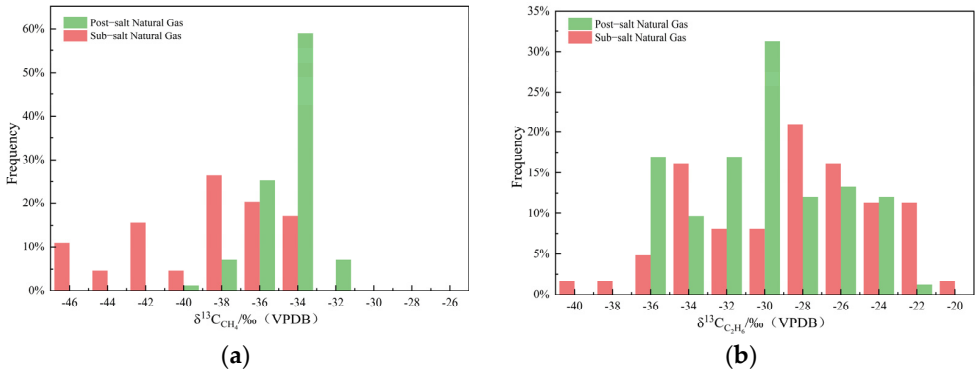

Figure 3. Frequency distributions map of the carbon isotope composition of alkanes in Ordovician carbonate gas in the Ordos Basin. (**a**) Frequency distribution of methane carbon isotope composition in natural gas. (**b**) Frequency distribution of ethane carbon isotope composition in natural gas.

The carbon isotope data of natural gas in the Lower Paleozoic strata of the Ordos Basin also showed a certain pattern with the changing in depth. The carbon isotope composition of natural gas methane gradually became heavier with increasing depth, but the carbon isotope composition of ethane and propane became heavier and then lighter with increasing depth. This may be a result of the joint action of maturity and type of parent material. Notably, the $\delta^{13}C$ of natural gas becomes lighter and then heavier with increasing maturity [36]. It is also possible that this natural gas was formed by secondary modification (Figure 4).

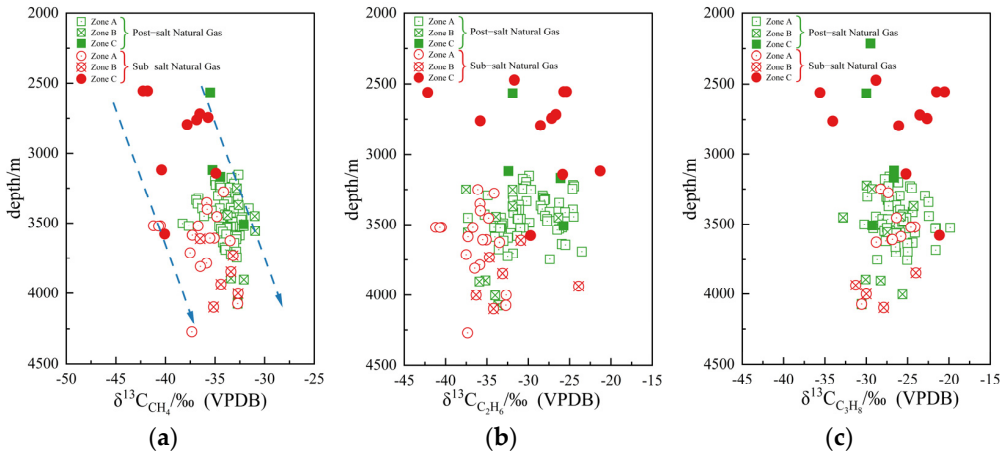

Figure 4. Carbon isotope signature versus depth plots for different natural gas components in Ordos Basin Ordovician carbonate facies. (**a**) Relationship between methane carbon isotope characteristics and depth of natural gas. (**b**) Relationship between ethane carbon isotope characteristics and depth of natural gas. (**c**) Relationship between propane carbon isotope characteristics and depth of natural gas.

5. Discussion

5.1. Comprehensive Identification of Genetic Types of Natural Gas in Ordovician Carbonate Strata

The carbon isotope composition of natural gas methane is affected by the type of parent material, degree of thermal evolution, and secondary transformation. It is usually affected by many factors over geological time, which may lead to deficiencies in the use of natural gas carbon isotope composition in genetic identification and gas source correlation. In particular, during the process of natural gas generation and accumulation in the Majiagou Formation, the gas has been modified by variable degrees of thermochemical sulfate reduction (TSR), resulting in substantial changes to the chemical and isotopic compositions of the natural gas. It is, therefore, difficult to draw conclusions consistent with geological reality using only the carbon isotope composition of natural gas methane as an index to analyze its genesis and gas source.

Methane–carbon and methane–hydrogen isotopic compositions are important parameters for determining the genesis and thermal evolution of natural gas [37,38]. It is generally inferred that the methane carbon isotope composition is mainly affected by the degree of thermal evolution of the hydrocarbon source rock, with a higher degree of thermal evolution equating to a heavier methane carbon isotope value. The ethane carbon isotope composition is strongly influenced by the original parent material; although it is also affected by the thermal evolution degree of the source rock, the effect is much smaller than the methane carbon isotope composition. Therefore, the ethane carbon isotope composition is often used as an effective index to distinguish coal-type gas from oil-type gas [39]. At present, domestic scholars mainly use −28‰ [40] or −29‰ [39] as the boundary value in China.

The methane carbon isotope composition of natural gas in the mature stage varies from −50‰ to −20‰, while the methane hydrogen isotope composition can vary from −250‰ to −150‰ [41]. Compared with carbon isotopes, hydrogen isotopes may be more responsive to geochemical changes in a given environment owing to their larger potential range and incremental changes in their composition. The hydrogen isotope composition of hydrocarbons has been investigated in a number of studies [42]. Methane hydrogen isotope compositions are mainly influenced by the parent material, aqueous environment at the time of natural gas formation, and degree of thermal evolution; they are governed first by the depositional environment and second by the degree of maturity.

Wang et al. (2015) [43] analyzed the carbon and hydrogen isotope compositions of methane in typical sedimentary basins in China and established an oil-type gas versus coal-type gas discrimination diagram. Their study showed that the hydrogen isotope compositions of natural gas components produced by hydrocarbon source rocks formed in freshwater environments are light, and conversely, those of natural gas components formed in saltwater environments are heavy. Their study also showed that natural gas methane carbon and hydrogen isotopes are positively correlated with increasing thermal maturity. In addition, the hydrogen isotope composition of typical marine humic natural gas is heavier than that of typical coal-type gas; the former is generally >−180‰, while the latter is only >−180‰ when the degree of thermal evolution is very high. The methane–hydrogen isotope composition of natural gas can be used to study the aqueous environment in which its parent material was deposited, enabling comparative natural gas–gas source rock studies [44]. The isotopic data from the natural gas samples in this study are plotted on a discrimination diagram (Figure 5), where they are plotted near the area of natural gas formed by marine humic organic matter, indicating an origin from Ordovician carbonate hydrocarbon source rocks. The “post-salt” natural gas samples were more dispersed between the coal-type and oil-type gas regions, showing mixed-source characteristics.

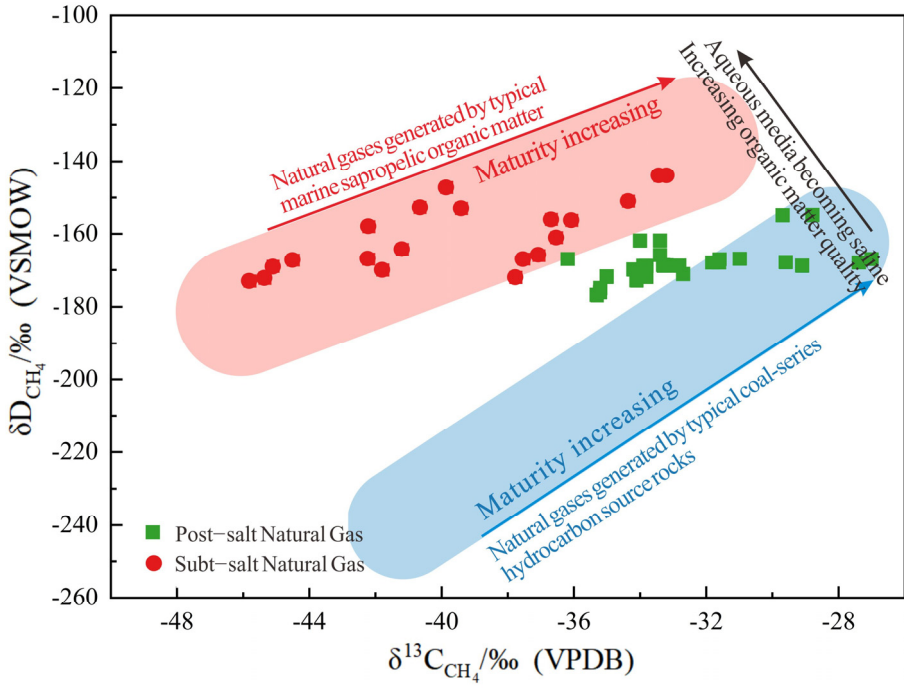

Figure 5. $\delta^{13}C_{CH4}-\delta D_{CH4}$ relationship of natural gas samples from Ordos Basin Ordovician carbonate facies.

The combination of hydrocarbon fraction ratios and carbon isotope compositions can also be used to classify the type of natural gas genesis. The Bernard diagram has been used to identify the type of natural gas genesis on the basis of a large number of natural gas sample datapoints [45]. Using this diagram, the "post-salt" natural gas parent material in the study area can be classed as a mixture of type II and type III kerogen but dominated by type II kerogen; in contrast, most of the "sub-salt" natural gas samples plotted in the type II kerogen region, this being the oil-type gas region (Figure 6).

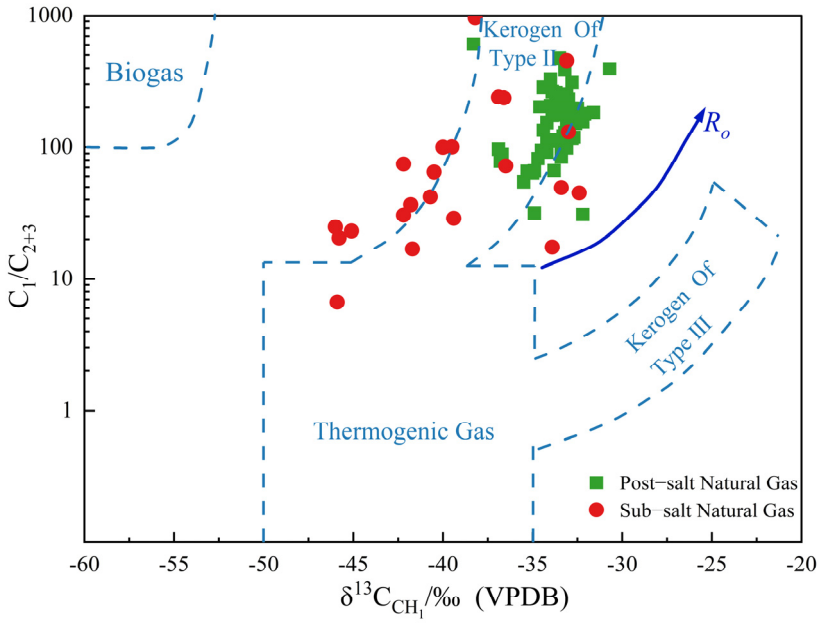

Figure 6. $\delta^{13}C_{CH4}-C_1/C_{2+3}$ relationship for natural gas samples in Ordos Basin Ordovician carbonate facies.

5.2. Carbon Isotope Anomalies in "Sub-Salt" Natural Gas

During the hydrocarbon evolution of sedimentary organic matter, there are kinetic fractionation and inheritance effects between natural gas components and parent carbon isotopes; lower carbon number hydrocarbons are more likely to be enriched in ^{12}C, and higher carbon number hydrocarbons are more likely to be enriched in ^{13}C. Thus, the carbon isotope composition of organogenic alkane gases tends to show the pattern $\delta^{13}C_{CH4} < \delta^{13}C_{C2H6} < \delta^{13}C_{C3H8}$ [46].

The inversion of alkane gas carbon isotope sequences often occurs under natural geological conditions, potentially caused by the mixing of natural gas of organic origin with natural gas of inorganic origin, mixing of oil-type gas with coal-type gas, mixing of homologous and non-homologous gas, or oxidation of natural gas by bacteria [23]. Such carbon isotope sequence inversions may result from a single cause or a combination of causes.

Chung (1988) [47] combined theoretical calculations of carbon isotope fractionation with simulation experiments and found that the alkane carbon isotope values of natural gas from a single source (which did not experience the effects of secondary modification) showed a decreasing trend with increasing carbon number, and were linearly related to the inverse of the alkane carbon number. However, most of the carbon isotope sequence diagrams of "sub-salt" natural gas samples are non-collinear, meaning that they may have mixed sources or may have undergone secondary reformation (Figure 7).

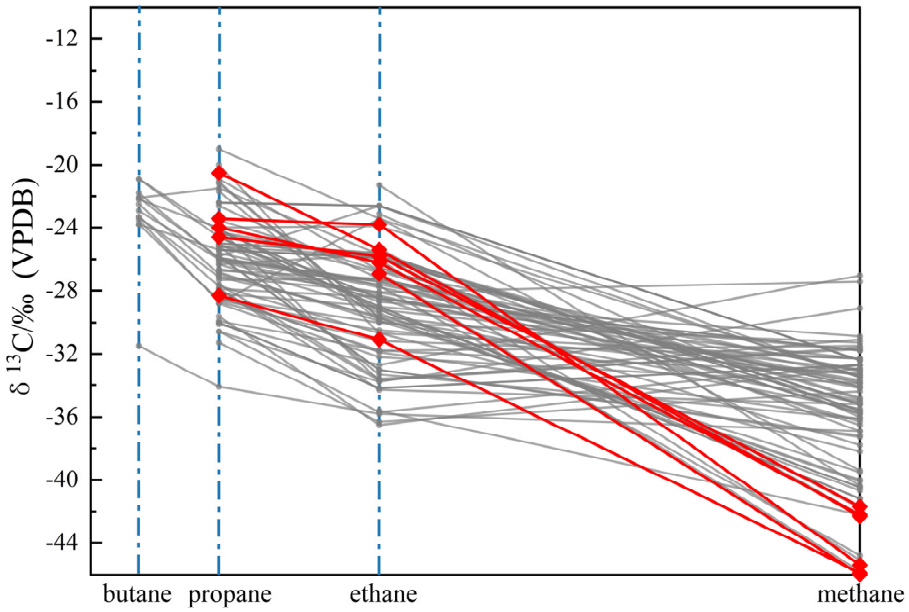

Figure 7. Carbon isotope sequence patterns of Ordos Basin Ordovician "sub−salt" natural gas.

Taking the "sub-salt" natural gas of the MT1 and M104 wells as an example, the carbon isotope compositions of the former are $\delta^{13}C_{CH4} = -45.4‰$, $\delta^{13}C_{C2H6} = -23.8‰$, and $\delta^{13}C_{C3H8} = -23.4‰$, while those of the latter are $\delta^{13}C_{CH4} = -41.8‰$, $\delta^{13}C_{C2H6} = -25.7‰$, and $\delta^{13}C_{C3H8} = -21.5‰$. These values are low compared with the $\delta^{13}C_{CH4}$ average value for "post-salt" natural gas of −33.8‰ and high compared with the average $\delta^{13}C_{C2H6}$ value of −30.0‰ for "post-salt" natural gas, showing their unique isotopic compositional characteristics. This is unlikely to have been caused by a mixed source because of the overlying well-separated gypsum layer with a thickness of up to 100 m, as well as the large vertical distance to the Upper Paleozoic coal hydrocarbon source rock; it would be immensely difficult for Upper Paleozoic coal-type gas to reflow into the "sub-salt" strata. Hence, we infer that the action of TSR has modified the "sub-salt" natural gas to form the present carbon isotope signature.

5.3. Natural Gas Secondary Rehabilitation: Exploration of TSR Mechanisms

Thermochemical sulfate reduction is a common organic–inorganic process in marine carbonate reservoirs. It specifically refers to the redox reaction between sulfate and hydrocarbons (organic matter) in formation with water, which generates CO_2 and H_2S; during this reaction, the hydrocarbon components and their carbon isotope compositions undergo a transformation process [48]. The reaction formula is: $CaSO_4$ + Hydrocarbons $\rightarrow$ $CaCO_3$ + H_2O + H_2S + S + CO_2 [49]. The formation of H_2S can be geochemically classified into three different mechanisms: biodegradation, high-temperature splitting of sulfide minerals, and TSR [50]. However, the first two mechanisms are limited by the reactive substances, and the volume fraction of H_2S will not be >4%; hence, TSR dominates in nature. The oil–water interface and TSR reaction during crude oil cracking and its secondary reformation in oil and gas reservoirs containing gypsum salt and carbonates have been studied in recent decades [51]. However, TSR reactions in carbonate hydrocarbon source rocks have not yet been addressed.

The "sub-salt" strata in the mid-eastern Ordos Basin experienced successive phases of sea transgression and regression, forming dolomitic mudstone, muddy dolomite, and high-quality dolomite with high organic matter abundance under the strongly reducing environment of the regressive phases. They also experienced deep burial, and at the same time, there is a shelter above the gypsum-salt rock, which is favorable for aggregation and formation. Hence, there were suitable material and energy conditions for TSR to occur during the process of hydrocarbon and reservoir formation [12].

The TSR reaction experienced by hydrocarbons in the Ordovician carbonate facies was an ongoing and complex process. According to the degree of thermal evolution and TSR reaction intensity, this process can be approximately divided into three stages (Figures 8 and 9): (1) macromolecular organic reaction stage; (2) gaseous heavy hydrocarbon reaction stage; and (3) methane reaction stage. The degree of TSR during stage (1) was relatively weak; as the reaction proceeded, macromolecular organic matter with lower activation energies reacted preferentially, the gas dried out, and the carbon isotope compositions of methane and ethane became progressively lighter in relation to the pyrolysis gas. This stage mainly occurred in zone B, where the thermal evolution degree was low, and the TSR reaction was weak. The heavy hydrocarbons gradually began to react in stage (2), with the carbon isotope composition of methane becoming lighter and those of ethane and other gaseous hydrocarbons becoming heavier. This stage mainly occurred in the eastern part of Zone A and western part of Zone B, which belong to the area of the Jingbian gasfield. During stage (3), as the TSR reaction proceeded further, the heavy hydrocarbon component was consumed, methane became the main reactant, and the carbon isotope compositions of both methane and ethane became heavier. This stage mainly occurred in areas with a strong TSR reaction, such as the T122 well in Zone A and MT1 well in Zone B. The content of hydrogen sulfide in natural gas in these zones is usually high, indicating a more complete TSR reaction.

Previous studies have found that the TSR process has a significant modifying effect on the chemical composition of natural gas. The thermochemical sulfate reduction will result in the preferential oxidization of heavy hydrocarbon gases, with methane being the most difficult to oxidize; this leads to natural gas with an H_2S content >10%, a dry coefficient increment of up to 99.9% [52], and even close to 1 corresponding to stage (1). When the reaction proceeds to stage (2) and begins to oxidize ethane, the preferential oxidation of $^{12}C_{C2H6}$ molecules results in an elevated proportion of $^{13}C_{C2H6}$ in the remaining ethane, equating to variations in $\delta^{13}C_{C2H6}$ of a few ‰ to a dozen ‰ [53]. At this time, the carbon isotope composition of ethane is heavier, which may correspond to the anomaly that some "sub-salt" natural gas appears to be favored. For example, $\delta^{13}C_{C3H8} = -23.4$‰. Cai et al. (2004) [54] found that TSR changes the drying factor from 0.996 to 0.9995 with a methane carbon isotope value of approximately 3‰. Corresponding to stage (3) in Figure 8, methane is not oxidized until the TSR reaction is almost complete; this stage affects the original

methane content and its carbon isotope composition, but this is not yet reflected in the natural gas of the MT1 well.

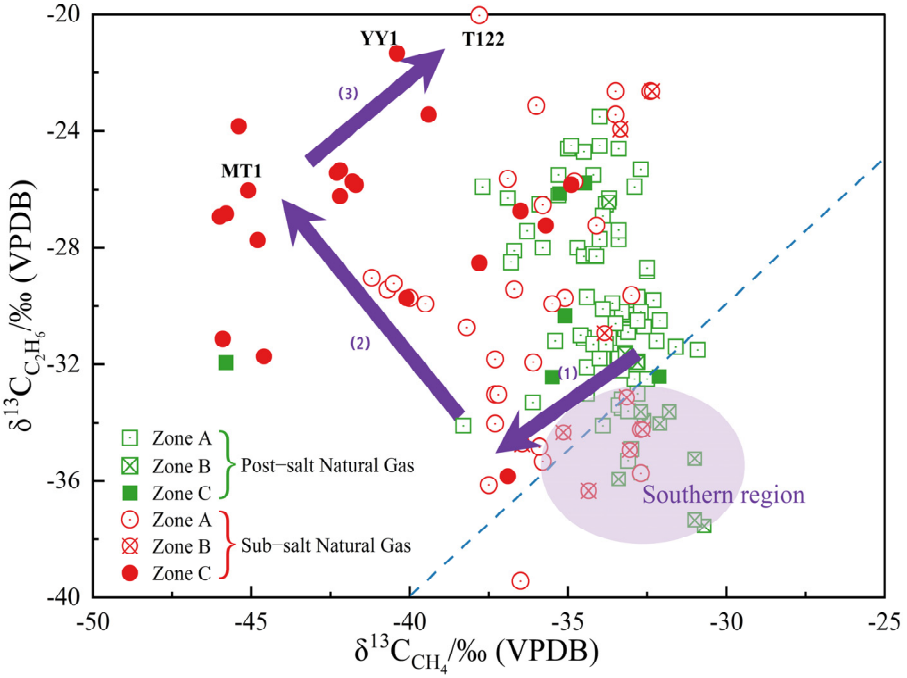

Figure 8. $\delta^{13}C_{CH4}-\delta^{13}C_{C2H6}$ relationship for natural gas samples from carbonate formations in the Ordos Basin.

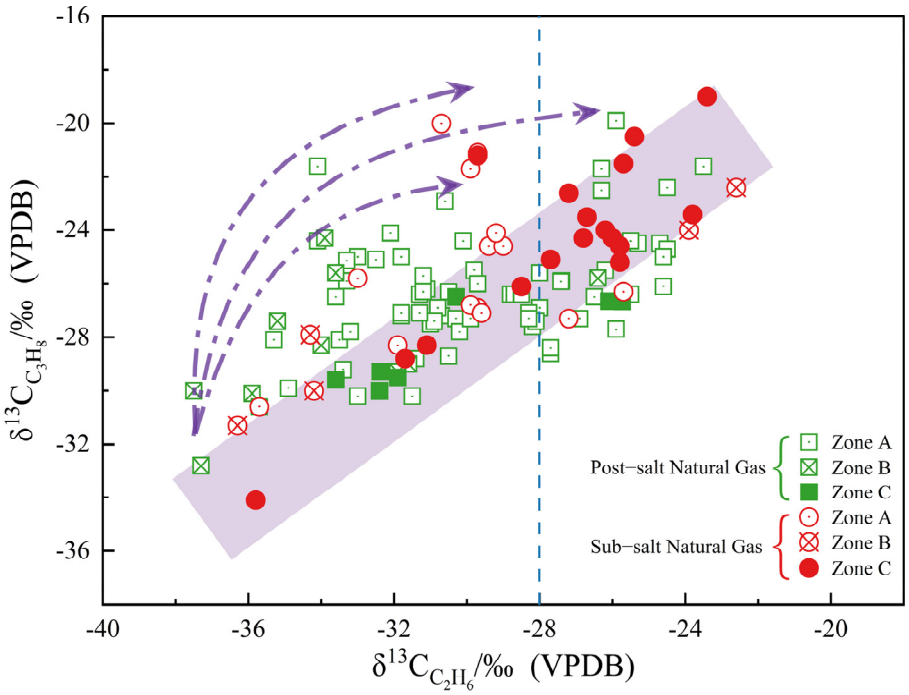

Figure 9. Model diagram of the effect of thermochemical sulfate reduction on the carbon isotope composition of natural gas.

Typically, a higher H_2S content equates to a stronger TSR effect, so the H_2S content can reflect the extent to which TSR has occurred. All Ordovician natural gas contains H_2S, but there is a substantial difference in the H_2S content between "post-salt" and "sub-salt" natural gas, with the former having a relatively low H_2S content (mean 0.09%), and the

latter having a much higher H_2S content (mean 9.51%) (Table 1). Notably, a low H_2S content does not necessarily equate to a weak TSR effect because the H_2S content is also related to its preservation; free H_2S can only occur after heavy metal ions in the reservoir are completely consumed via the formation of stable metal sulfides. This occurs after the formation of water solubility saturation. Sulfur in the "post-salt" natural gas is probably retained in the form of pyrite. In contrast, large quantities of H_2S gas are formed in "sub-salt" strata during the TSR reaction process and are preserved in "sub-salt" reservoirs with good containment properties, forming the high sulfur gas reservoirs observed today.

5.4. The Influence of TSR on Exploration and Development

Thermochemical sulfate reduction is a process in which hydrocarbons react with sulfates to reduce sulfate minerals and produce acidic gases, such as H_2S and CO_2, under the driving power of heat. Sulfate ions, hydrocarbons, and high temperatures provide the necessary materials and thermodynamic conditions for the occurrence of TSR [55]. Elemental sulfur and H_2S can be used as catalysts to increase the reaction rate of TSR. The H_2S and CO_2 produced by the TSR reaction dissolve in the formation of water to form acidic fluids, and the organic–inorganic interactions within carbonate reservoirs are able to dissolve certain parts of said reservoirs [56]. This will impact later exploration and development.

During the process of exploration and development, oil- and gas-source correlation research will be carried out, and natural gas isotope composition will likely be used as an important discriminant index. However, TSR can change the isotopic composition of natural gas, and different stages of the reaction produce different types of effects, leading to errors in oil- and gas-source correlation studies. Knowledge of whether natural gas has undergone TSR and the extent of this reaction means that the original isotopic composition of the natural gas can be determined, and oil and gas sources can be studied in more detail. In this paper, we have further clarified the TSR reaction process by studying the causes of heavy hydrocarbon carbon isotope anomalies in marine carbonate gas; this research also provides a theoretical basis for the subsequent exploration and development of natural gas.

6. Conclusions

The object of this study was to clarify the genetic types and sources of Lower Paleozoic (Ordovician) "sub-salt" natural gas in the mid-eastern Ordos Basin. We analyzed the organic components and carbon and hydrogen isotope signatures of 155 Ordovician natural gas samples from the mid-eastern Ordos Basin, and the differences between Upper Paleozoic and Lower Paleozoic natural gas samples were compared and discussed. The study focused on the similarities, differences, and possible causes of natural gas above and below the Majiagou Formation in different regions, highlighted the role of the hydrogen isotope composition of natural gas in genesis and gas-source identification, and systematically analyzed the influence of TSR on carbon isotope composition during the formation and accumulation of natural gas. The main conclusions are as follows:

(1) There were evident anomalies between the geochemical characteristics of Ordovician "sub-salt" and "post-salt" natural gas, with the former having a larger range of methane content compared with the latter, but the ethane content was lower and had a smaller range of variation. In general, the methane carbon isotope composition of the "sub-salt" natural gas was lighter than that of the "post-salt" natural gas; the ethane carbon isotope composition of the "sub-salt" natural gas was more widely distributed and partly lighter than that of the "post-salt" natural gas.

(2) The Ordovician "post-salt" natural gas is a composite of Upper Paleozoic coal-type gas and Lower Paleozoic oil-type gas, with the oil-type gas accounting for a larger contribution. In contrast, the "sub-salt" natural gas was formed and preserved within the Ordovician marine carbonates or sourced from deeper and more ancient hydrocarbon source rocks.

(3) The Ordovician "sub-salt" hydrocarbon source rocks and reservoirs in the mid-eastern part of the Ordos Basin are rich in anhydrite and have generally experienced large burial depths, possessing the material and energy conditions for the occurrence of TSR; they have generally experienced TSR during the process of hydrocarbon formation and reservoir formation. This has affected the carbon isotope composition of the "subsalt" natural gas, leading to anomalously light methane carbon isotope signatures and anomalously heavy ethane carbon isotope signatures.

Author Contributions: Conceptualization, W.L.; formal analysis, W.Z.; investigation, W.Z. and H.L.; data curation, W.Z.; writing—original draft preparation, W.Z.; writing—review and editing, W.L., H.L. and P.L.; supervision, X.W., D.Z. and X.C.; project administration, Z.H., Q.K. and Z.C. All authors have read and agreed to the published version of the manuscript.

Funding: This study was financially sponsored by the National Natural Science Foundation of China (Grant No. 41930426 and No. 42172173) and the PetroChina Changqing Oilfield Company, Science and Technology Major Project (Grant No. ZDZX2021-03).

Institutional Review Board Statement: Not applicable.

Informed Consent Statement: Not applicable.

Data Availability Statement: The data supporting the research results obtained from the National Natural Science Foundation of China; the PetroChina Changqing Oilfield Company, Science and Technology Major Project, but the availability of these data is limited. These data are used under the permission for the current research, so they are not disclosed.

Conflicts of Interest: The authors declare no conflict of interest.

References

1. Li, J.Z.; Tao, X.W.; Bai, B.; Huang, S.P.; Jiang, Q.C.; Zhao, W.Y.; Chen, Y.Y.; Ma, D.B.; Zhang, L.P.; Li, N.X.; et al. Geological conditions, reservoir evolution and favorable exploration directions of marine ultra-deep oil and gas in China. *Pet. Explor. Dev.* **2021**, *48*, 60–79. [CrossRef]
2. He, Z.X.; Zheng, C.B.; Wang, C.L.; Huang, D.J. Cases of Discovery and Exploration of Marine Fields in China (Part 2): Jingbian Gas Field, Ordos Basin. *Mar. Petrol. Geol.* **2005**, *10*, 37–44.
3. Guo, Y.R.; Fu, J.H.; Wei, X.S.; Xu, W.L.; Sun, L.Y.; Liu, J.B.; Zhao, Z.Y.; Zhang, Y.Q.; Gao, J.R.; Zhang, Y.L. Natural gas accumulation and models in Ordovician carbonates, Ordos Basin, NW China. *Pet. Explor. Dev.* **2014**, *41*, 437–448. [CrossRef]
4. Fu, J.H.; Yu, Z.; Li, C.S.; Wang, W.B.; Huang, Z.L.; Wu, X.N.; Wang, S.Y. New discovery and favorable areas of natural gas exploration in the 4th Member of Ordovician Majiagou Formation by Well Mitan 1 in the eastern Ordos Basin. *Nat. Gas. Ind. B* **2021**, *41*, 17–27. [CrossRef]
5. Liu, D.; Zhang, W.Z.; Kong, Q.F.; Feng, Z.Q.; Fang, C.C.; Peng, W.L. Lower Paleozoic source rocks and natural gas origins in Ordos Basin, NW China. *Pet. Explor. Dev.* **2016**, *43*, 591–601. [CrossRef]
6. Cao, H.X.; Wang, N.X.; Qiang, J.; Wu, H.Y.; Shang, T. Natural gas reservoir forming conditions about Lower Paleozoic carbonate. *J. Xi'an Univ. Sci. Technol.* **2014**, *34*, 713–718. [CrossRef]
7. Ran, X.Q.; Fu, J.H.; Wei, X.S.; Ren, J.F.; Sun, L.Y.; Bao, H.P. Evolution of the Ordovician top boundary and its relationship to reservoirs' development, Ordos Basin. *Pet. Explor. Dev.* **2012**, *39*, 165–172. [CrossRef]
8. Fu, J.H.; Liu, X.S.; Wei, L.B.; Ren, J.F.; Gu, Y.H.; Wang, Q.P.; Shi, P.P. Breakthrough and significance of natural gas exploration in the fourth member of Majiagou Formation of subsalt Ordovician in Ordos Basin. *China Pet. Explor.* **2022**, *27*, 47–58.
9. Bao, H.P.; Wang, Q.P.; Yan, W.; Cai, Z.H.; Zheng, J.; Wei, L.B.; Huang, Z.L.; Guo, W. Sedimentary characteristics and gas accumulation potential of the Ordovician carbonate evaporate paragenesis system in central and eastern Ordos Basin. *Earth Sci. Front.* **2023**, *30*, 30–44. [CrossRef]
10. Li, J.; Li, J.; Li, Z.S.; Zhang, C.L.; Cui, H.Y.; Zhu, Z.L. Characteristics and genetic types of the Lower Paleozoic natural gas, Ordos Basin. *Mar. Pet. Geol.* **2018**, *89*, 106–119. [CrossRef]
11. Zhao, W.Z.; Bian, C.S.; Xu, Z.H. Similarities and differences between natural gas accumulations in Sulige gas field in Ordos basin and Xujiahe gas field in Central Sichuan Basin. *Pet. Explor. Dev.* **2013**, *40*, 429–438. [CrossRef]
12. Liu, W.H.; Wang, X.F.; Zhang, D.D.; Cai, Z.H.; Luo, H.Y.; Chen, X.Y.; Wang, T.; Li, F.R.; Zhang, W.; Li, F.Q. Restudy on geochemical characteristics and genesis of Jingbian Gas Field in Ordos Basin. *J. Northwest Univ.* **2022**, *52*, 943–956. [CrossRef]
13. Yang, H.; Liu, X.S. Progress in Paleozoic coal-derived gas exploration in the Ordos Basin, West China. *Pet. Explor. Dev.* **2014**, *41*, 144–152. [CrossRef]

14. Wang, G.T.; Cheng, L.H.; Meng, D.W.; Zhu, Y.J.; Sun, J.W.; Huang, J.X.; Peng, Y.X. Characterization and formation of the Ordovician tight paleokarst carbonates in the eastern Ordos Basin and its gas accumulation. *Oil. Gas. Geol.* **2018**, *39*, 685–695. [CrossRef]
15. Bao, H.P.; Yang, C.Y.; Huang, J.S. "Evaporation drying " and "reinfluxing and redissolving"—A new hypothesis concerning formation of the Ordovician evaporites in eastern Ordos Basin. *J. Palaeogeogr.* **2004**, *6*, 279–288.
16. Di, X.; Tan, X.C.; Zhang, D.F.; He, W.; Li, L.; Shi, Y.H.; Chen, J.P.; Cao, J. Discovery of syngenetic and eogenetic karsts in the Middle Ordovician gypsum-bearing dolomites of the eastern Ordos Basin (central China) and their heterogeneous impact on reservoir quality. *Mar. Pet. Geol.* **2019**, *99*, 190–207. [CrossRef]
17. Zhou, J.G.; Yin, C.; Zeng, L.B.; Hi, C.; Wu, D.X.; Yu, Z.; Li, W.L.; Tang, J.; Liu, Y.X.; Jia, J.J. Development characteristics of grain shoals and favorable gas exploration areas in the 4th Member of Ordovician Majiagou Formation in the Ordos Basin. *Nat. Gas. Ind. B* **2022**, *42*, 17–30.
18. Hu, G.; Liu, W.H.; Luo, H.Y.; Wang, J.; Chen, Q.L.; Borjigin, T.; Lu, L.F. The Impaction of Original Organism Assemblages in Source Rocks on the Kerogen Carbon Isotopic Compositions: A Case Study of the Early Paleozoic Source Rocks in the Tarim Basin, China. Bulletin of Mineralogy. *Petrol. Geochem.* **2019**, *38*, 902–913+869. [CrossRef]
19. Fu, J.H.; Wu, X.N.; Sun, L.Y.; Yu, Z.; Huang, Z.L.; Ding, Z.C. New understandings of the lithofacies paleogeography of the middle assemblage of Majiagou Fm in the Ordos Basin and its exploration significance. *Nat. Gas. Ind. B* **2017**, *4*, 278–286. [CrossRef]
20. Yu, J.; Ma, T.; Miao, Q.H.; Song, J. Analysis of Components in Refinery Gas by Agilent 7890A Gas Chromatograph. *Contemp. Chem. Ind.* **2015**, *44*, 1179–1181. [CrossRef]
21. He, X.L.; Liu, C.L.; Wang, J.T.; Zhang, Y.Y.; Meng, Q.G. Measurement of carbon and hydrogen isotopes of natural gas hydrate-bound gases by gas chromatography-isotope ratio mass spectrometry. *Rock. Miner. Test.* **2012**, *31*, 154–158.
22. Dai, J.X.; Li, J.; Ding, W.W.; Hu, G.Y.; Luo, X.; Tao, S.Z.; Zhang, W.Z.; Zhu, G.Y.; Mi, J.K. Geochemical characters of the giant gas accumulations with over one hundred billion cubic meters reserves in China. *Pet. Explor. Dev.* **2005**, *4*, 16–23.
23. Dai, J.X.; Zou, C.N.; Liao, S.M.; Dong, D.Z.; Ni, Y.Y.; Huang, J.L.; Wu, W.; Gong, D.Y.; Huang, S.P.; Hu, G.Y. Geochemistry of the extremely high thermal maturity Longmaxi shale gas, southern Sichuan Basin. *Org. Geochem.* **2014**, *74*, 3–12. [CrossRef]
24. Yang, H.; Zhang, W.Z.; Zan, C.L.; Ma, J. Geochemical Characteristics of Ordovician Subsalt Gas Reservoir and Their Significance for Reunderstanding the Gas Source of Jingbian Gasfield East Ordos Basin. *Nat. Gas Geosci.* **2009**, *20*, 8–14.
25. Yang, H.; Liu, X.S.; Yan, X.X.; Zhang, H. The Shenmu Gas Field in the Ordos Basin: Its discovery and reservoir forming geological characteristics. *Nat. Gas Ind.* **2015**, *35*, 1–13. [CrossRef]
26. Liu, Q.Y.; Chen, M.J.; Liu, W.H.; Li, J.; Han, P.L.; Guo, Y.R. Origin of natural gas from the Ordovician paleo-weathering crust and gas-filling model in Jingbian Gas Field, Ordos Basin, China. *J. Asian Earth Sci.* **2009**, *35*, 74–88. [CrossRef]
27. Liu, Q.Y.; Jin, Z.J.; Meng, Q.Q.; Wu, X.Q.; Jia, H.C. Genetic types of natural gas and filling patterns in Daniudi gas field, Ordos Basin, China. *J. Asian Earth Sci.* **2015**, *107*, 1–11. [CrossRef]
28. Xiao, H.; Zhao, J.Z.; Wang, D.X.; Ren, J.F.; Ma, Z.R.; Wu, W.T. Geochemical characteristics of primary gas in the Ordovician and their significance for the gas source of Jingbian Gas Field, Ordos Basin. *Oil Gas Geol.* **2013**, *34*, 601–609.
29. Zhang, W.Z.; Yang, H.; Zan, C.L.; Kong, Q.F. Geochemical study of paleozoic gas reservoirs in a highly mature area on the south-central Yishan slope, Ordos Basin. *Geochimica* **2016**, *45*, 614–622.
30. Wang, K.; Pang, X.Q.; Zhao, Z.F.; Wang, S.; Hu, T.; Zhang, K.; Zheng, T.Y. Geochemical characteristics and origin of natural gas in southern Jingbian gas field, Ordos Basin, China. *J. Nat. Gas Sci. Eng.* **2017**, *46*, 515–525. [CrossRef]
31. Hu, A.P.; Li, J.; Zhang, W.Z.; Li, Z.S.; Hou, L.; Liu, Q.Y. Geochemical characteristics and genetic types of natural gas in Upper, Lower Paleozoic and Mesozoic in Ordos Basin. *Sci. China (Ser. D Earth Sci.)* **2007**, *37*, 157–166.
32. Kong, Q.F.; Zhang, W.Z.; Li, J.F.; Zan, C.L. Geochemical characteristics and genesis of Ordovician natural gas under gypsolyte in Ordos Basin. *Nat. Gas Geosci.* **2019**, *30*, 423–432.
33. Xu, W.L.; Hu, S.Y.; Li, N.X.; Wei, X.S.; Gao, J.R.; Zhao, Z.Y.; Li, X.B.; Liu, J.B.; Zhang, Y.Q.; Song, H. Characteristics and exploration directions of inner gas source from the middle assemblage of Ordovician in Ordos Basin. *Acta Pet Sin.* **2019**, *40*, 900–913.
34. Liu, E.H.; Chen, Z.P.; Wang, Q.C.; Bai, N.; Li, J.; Liao, Y. Genetic types of natural gas from upper & middle assemblage of Majiagou Formation in Jingbian area, Ordos Basin. *J. Xi'an Univ. Sci. Technol.* **2022**, *42*, 324–334. [CrossRef]
35. Meng, Q.; Shi, J.L.; Zhao, H.; Huang, J.P.; Liu, Y.; Wang, J.Q.; Xie, X.M.; Xu, Y.H. Genesis and source of natural gas in Well Mitan-1 of Ordovician Majiagou Formation, middle-eastern Ordos Basin. China. *Nat. Gas Geosci.* **2023**, *34*, 1696–1709.
36. Chen, L.; Zheng, L.J.; Huang, H.P.; Ning, C.X. Carbon isotopic evolution of hydrocarbon gases generated from carbonate source rocks via thermal simulation methods. *Pet. Geol. Exp.* **2021**, *44*, 121–128+138.
37. Schiell, M. The hydrogen and carbon isotopic composition of methane from natural gases of various origins. *Geochim. Cosmochim. Acta* **1980**, *44*, 649–661. [CrossRef]
38. Whhiticar, M.J. Carbon and hydrogen isotope systematics of bacterial formation and oxidation of methane. *Chem. Geol.* **1999**, *164*, 291–314. [CrossRef]
39. Dai, J.X.; Xia, X.Y.; Li, Z.S.; Dennis, D.C.; Rpbert, F.D.; Gao, L.; Li, J.; Daniel, D.; Dominique, D.; Li, L.W.; et al. Inter-laboratory calibration of natural gas round robins for δ2H and δ13C using off-line and on-line techniques. *Chem. Geol.* **2012**, *310–311*, 49–55. [CrossRef]
40. Chen, J.F.; Li, C.G.; Shen, P.; Ying, G.G. Carbon and hydrogen isotopic characteristics of hydrocarbons in coal type gas from China. *Acta Sedimentae Sin.* **1995**, *13*, 59–69.

41. Ni, Y.Y.; Ma, Q.S.; Ellis, G.S.; Dai, J.X.; Katz, B.; Zhang, S.C.; Tang, Y.C. Fundamental studies on kinetic isotope effect (KIE) of hydrogen isotope fractionation in natural gas systems. *Geochim. Cosmochim. Acta* **2011**, *75*, 2696–2707. [CrossRef]
42. Tang, Y.C.; Huang, Y.S.; Ellis, G.S.; Wang, Y.; Kralert, P.G.; Gillaizeau, B.; Ma, Q.S.; Hwang, R. A kinetic model for thermally induced hydrogen and carbon isotope fractionation of individual n-alkanes in crude oil. *Geochim. Cosmochim. Acta* **2005**, *69*, 4505–4520. [CrossRef]
43. Wang, X.F.; Liu, W.H.; Shi, B.G.; Zhang, Z.N.; Xu, Y.C.; Zheng, J.J. Hydrogen isotope characteristics of thermogenic methane in Chinese sedimentary basins. *Org. Geochem.* **2015**, *83–84*, 178–189. [CrossRef]
44. Qi, Y.L. Method and application of hydrogen isotope analysis of nalkanes. *Pet. Geol. Exp.* **2020**, *42*, 319–324.
45. Bernard, B.B.; Brooks, J.M.; Sackett, W.M. Light hydrocarbons in recent Texas continental shelf and slope sediments. *J. Geophys. Res.* **1978**, *83*, 4053–4061. [CrossRef]
46. Dai, J.X.; Zou, C.N.; Zhang, S.C.; Li, J.; Ni, Y.Y.; Hu, G.Y.; Luo, X.; Tao, S.Z.; Zhu, G.Y.; Mi, J.K.; et al. Identication of inorganic origin and biogenie hydrocarbon gas. *Sci. China. Ser. D* **2008**, *38*, 1329–1341.
47. Chung, H.M.; Gormly, J.R.; Squires, R.M. Origin of gaseous hydrocarbons in subsurface environments: Theoretical considerations of carbon isotope distribution. *Chem. Geol.* **1988**, *71*, 97–103. [CrossRef]
48. Jiang, L.; Worden, R.H.; Cai, C.F. Generation of isotopically and compositionally distinct water during thermochemical sulfate reduction (TSR) in carbonate reservoirs: Triassic Feixianguan Formation, Sichuan Basin, China. *Geochim. Cosmochim. Acta* **2015**, *165*, 249–262. [CrossRef]
49. Shen, C.C.; Lu, H.; Hao, A.S.; Wang, Q.T.; Liu, D.Y. Differences in TSR behavior between n-heptane and toluene in simulation experiments. *Geochemistry* **2017**, *46*, 168–177. [CrossRef]
50. Yuan, Y.Y.; Wang, T.K.; Cai, C.F.; Xu, C.L.; Qin, Q.R. Relationships between sulfur-containing compound types in crude oil and Thermochemical Sulphate Reduction in Tazhong area. *J. Southwest Pet. Univ. (Sci. Technol. Ed.)* **2020**, *42*, 48–60. [CrossRef]
51. Ma, Y.S.; Guo, T.L.; Zhu, G.Y.; Cai, X.Y.; Xie, Z.Y. Evidence from simulation experiment of dissolution and reformation of hydrogen sulfide on carbonate reservoirs: Taking Feixianguan Formation in eastern Sichuan as an example. *Chin. Sci. Bull.* **2007**, *52*, 136–141. [CrossRef]
52. Cai, C.F.; Xiao, Q.L.; Fang, C.C.; Wang, T.K.; He, W.X.; Li, H.X. The effect of thermochemical sulfate reduction on formation and isomerization of thiadiamondoids and diamondoids in the Lower Paleozoic petroleum pools of the Tarim Basin, NW China. *Org. Geochem.* **2016**, *101*, 49–62. [CrossRef]
53. Mankiewicz, P.J.; Pottorf, R.J.; Kozar, M.G. Gas geochemistry of the mobile Bay Jurassic Norphlet Formation: Thermal controls and implications for reservoir connectivity. *AAPG Bull.* **2009**, *93*, 1319–1346. [CrossRef]
54. Cai, C.F.; Xie, Z.Y.; Worden, R.H.; Hu, G.Y.; Wang, L.S.; He, H. Methane-dominated thermochemical sulphate reduction in the Triassic Feixianguan Formation East Sichuan Basin, China: Towards prediction of fatal H2S concentrations. *Mar. Pet. Geol.* **2004**, *21*, 1265–1279. [CrossRef]
55. Liu, Q.; Lu, X.S.; Fan, J.S.; Liu, S.B.; Ma, X.Z.; Dai, B.K.; Gui, L.L.; Chen, W.Y. Evidence and controlling factors of thermochemical sulfate reduction in the Sinian gas reservoirs, Sichuan Basin. *Nat. Gas Geosci.* **2022**, *33*, 929–943.
56. Zhang, S.C.; Zhu, G.Y.; He, K. The effects of thermochemical sulfate reduction on occurrence of oil-cracking gas and reformation of deep carbonate reservoir and the interaction mechanisms. *Acta Petrol. Sin.* **2011**, *27*, 809–826.